Research article

X-RAY SPECTROMETRY

Received: 26 August 2014 Revised: 9 December 2014 Accepted: 9 December 2014 Published online in Wiley Online Library: 13 January 2015

(wileyonlinelibrary.com) DOI 10.1002/xrs.2580

Determination of the detection efficiency of a planar HPGe detector with a non-uniform frontal dead layer†

Lorenzo Brualla,[a]* Nora L. Maidana[b] and Vito R. Vanin[b]

Peak efficiency of a non-uniform frontal dead layer planar detector was simulated with the general purpose Monte Carlo radiation transport code PENELOPE. In a previous publication, using experimental data and an analytical model proposed by Seltzer, we found the structure and dimensions of the detectors dead layer. In this work, we used our previous results as input for a Monte Carlo simulation that considered a point source emitting specific photons from 13 to 122 keV, with the energies and emission probabilities of ^{241}Am, ^{133}Ba, ^{207}Bi, ^{57}Co, ^{137}Cs, and ^{152}Eu calibration sources, placed at 30 cm from the frontal surface of the detector. The geometry consisted of an amorphous Germanium cylinder, 2.5 cm in diameter and 1.0-cm thick, a 0.025-cm thick Be window and a 50-μm Al foil used in the experimental setup for irradiations in the Microtron de São Paulo. The simulation model succeeded as well as the analytical model and can be applied to other arrangements. **Copyright © 2015 John Wiley & Sons, Ltd.**

Introduction

The dead layers in HPGe detectors can become thicker during their lifetime. Furthermore, in a previous publication,[1], we observed that the thickness of the frontal dead layer of a 5 cc planar detector was not constant. In that publication, the thickness was determined by two procedures: (i) mapping the frontal surface with 0.1 and 0.2 cm aperture collimators over a grid of 0.3 × 0.3 cm^2 with 14 and 59 keV photons from an ^{241}Am calibration source; (ii) fitting by the least square method with an analytical efficiency model[2] for the full-energy absorption peaks at large source-to-detector distance.

Monte Carlo simulations of radiation transport have been successfully used in the past as an alternative method to determine the detection efficiency or the response function of HPGe detectors.[3–6] Usually, employing the nominal dimensions of the detector provided by the manufacturer in the simulated geometry yields detection efficiencies that are not compatible with the experimental observations. Researchers modify either the crystal dimensions or the dead layer thicknesses, or both, until simulation reaches an agreement with experiment. The initial geometry model usually employs the nominal dimensions and in a succession of simulations the dimensions are varied. This process is time-consuming because it is performed by trial and error, and each trial requires a set of simulations.

In this article, we refine the simulation process described earlier for finding the dead layer thickness of a HPGe detector. Our approach consists of using, as initial geometry model, the non-uniform frontal dead layers obtained in our previous publication,[1] derived from the Seltzer model.[2] With a reduced number of simulations, we were able to identify the thickness of the dead layers that reproduce the experimental data.

Experimental setup

A planar HPGe 5 cc detector (ORTEC, 1000 series low energy photon spectrometer) was used to measure cross sections for the ionization of the K shell by electrons at the São Paulo Microtron Accelerator (Instituto de Física da Universidade de São Paulo, Brazil).[7]

For the efficiency calibration, we used the following sources: ^{133}Ba, ^{152}Eu, ^{207}Bi, and ^{241}Am purchased from Amersham, and ^{57}Co and ^{137}Cs from Laboratório de Metrologia Nuclear-Instituto de Pesquisas Energéticas e Nucleares, Comissão Nacional de Energia Nuclear, São Paulo. The full-energy peak efficiency was determined with the energies of Table 1. The sources were mounted on an aluminum holder, which was placed at the center of an irradiation chamber, with a 50-μm thick aluminum window. The detector, placed outside the irradiation chamber, viewed the photons emitted from the sources at a distance of 29.95(10) cm from the frontal surface of the crystal.

Monte Carlo simulation

The general-purpose radiation transport Monte Carlo code PENELOPE[9–11] was used to simulate the response of the detector. PENELOPE contains a set of subroutines, which describe the coupled transport of photons, electrons, and positrons in material

* *Correspondence to: Lorenzo Brualla, NCTeam, Strahlenklinik, Universitätsklinikum Essen. Hufelandstraße 55, D-45122 Essen, Germany. E-mail: lorenzo.brualla@uni-due.de*

† *Presented at the European X-Ray Spectrometry Conference, Bologna, Italy, 15-20 June 2014.*

a *NCTeam, Strahlenklinik, Universitätsklinikum Essen., Hufelandstraße 55, D-45122 Essen, Germany*

b *Instituto de Física, Universidade de São Paulo. Travessa R 187, Cidade Universitária. CEP:05508-900 São Paulo, Brazil*

Copyright © 2015 John Wiley & Sons, Ltd.

Table 1. Photon energies (keV) considered for the simulation of each isotope

^{241}Am	^{133}Ba	^{207}Bi	^{57}Co	^{137}Cs	^{152}Eu
13.928^x	30.860^x	72.8049^x	14.41295	32.0610^x	39.91^x
26.3446	35.173^x	74.97^x	122.0607	36.5670^x	45.68^x
59.5409	53.1622	84.937^x	136.4736		121.7817
	80.89	87.58^x			

The energy data were taken from Bé et al.[8]
The energy uncertainties are in the last significant figure.
The superscript *x* indicates the x-rays, whose energies were computed as the average of the Kα and Kβ energies weighted with their relative intensities.

systems. The geometrical description of the media is carried out using bodies limited by quadric surfaces (planes, cylinders, etc.) Photon interactions are simulated one-by-one in chronological order, that is, in a detailed manner. Charged particles can either be simulated following this detailed approach, or using multiple scattering theories, in order to increase the simulation speed. In this latter approach, hard events, defined as those involving angular deflections or energy losses above certain cutoffs, are simulated in a detailed way. All soft collisions encountered between two hard interactions are lumped together, and they are described by a single artificial event. The cutoffs are determined by five user-defined transport parameters: `C1`, `C2`, `WCC`, `WCR`, and `DSMAX`. The average angular deflection caused by all elastic collisions in a path length equal to $\lambda_{el}^{(hard)}$, the mean free path between hard elastic collisions, is $1 - \exp(-C1) \simeq C1$ (typical values are in the interval $[0, 0.1]$). This is to say, `C1` determines $\lambda_{el}^{(hard)}$ and, therefore, the cutoff angle θ_c used to classify elastic events in the hard and soft categories. `C2` is the maximum fractional energy loss allowed in a single step. `WCC` and `WCR` are the cutoff energies for inelastic and bremsstrahlung interactions, respectively. `DSMAX` is an upper limit for the step length. All particles are transported until their kinetic energies fall below certain user-defined absorption energies `EABS`. Because PENELOPE is a set of subroutines, it requires a main steering program that, among other tasks, defines the source of particles and the quantities of interest to be scored. To that purpose, the code PENEASY[12] was used.

The detector was simulated as a cylinder made of amorphous germanium with a density $\rho = 5.323$ g/cm^3. The height of the cylinder was $h = 1$ cm and its radius $r = 1.25$ cm. Three dead layer regions were defined inside the cylinder:

1. A cylindrical frontal dead layer covering the upstream surface of the detector. The height of this dead layer is h_1 and its radius r_1.
2. A toroidal dead layer with rectangular cross section located in contact with the frontal dead layer, downstream of it. Its height is h_2. Its inner radius is r_2 and the outer radius 1.25 cm.
3. A toroidal dead layer with rectangular cross section located in contact with the previous one and downstream of it. Its height is h_3, that is, it spanned from the other toroidal dead layer until the downstream end of the detector. Its inner radius is r_3 and the outer radius 1.25 cm.

The detector geometry is depicted in Fig. 1. Table 2 reports the values defining the dead layer thicknesses obtained from the Seltzer model[1] and the simulation model found as described in the succeeding text.

All simulations included the detector beryllium ($\rho = 1.848$ g/cm^3) window of thickness 0.025 cm, which was placed in front of the detector. The upstream surface of the window was 0.6 cm away from the upstream surface of the detector. An aluminum ($\rho = 2.6989$ g/cm^3) window of thickness 50 μm was also placed in front of the detector with its upstream surface 11.1 cm from the upstream surface of the detector. This aluminum window corresponded to the vacuum seal of the irradiation chamber. Both windows were perpendicular to the symmetry axis of the detector. Also, both windows were sufficiently large in the perpendicular plane to the symmetry axis so to fully cover the detector as viewed from the source.

The point-like source was simulated to emit photons in a cone with semi-aperture $\theta_{sa} = 2.5°$ pointing in the direction normal to the frontal surface of the detector. This aperture illuminated the whole frontal surface of the detector, giving a wide margin. The source was placed on the symmetry axis of the detector, 29.95 cm away from its upstream surface. This simulated geometry reproduced the experimental setup.

Initially, six simulations were run using the dimensions obtained from the previous work (Table 2, 'previous' column), one for each of the following isotopes: ^{241}Am, ^{133}Ba, ^{207}Bi, ^{57}Co, ^{137}Cs and ^{152}Eu. Only photons with energies in Table 1 were simulated,

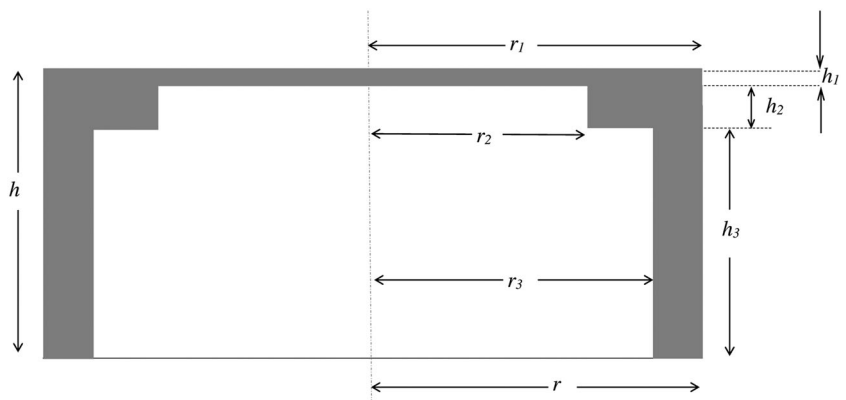

Figure 1. Sketch, not to scale, of the simulated crystal, cut through a plane along its cylindrical symmetry axis. The active volume and dead layers are white and dark gray, respectively.

Copyright © 2015 John Wiley & Sons, Ltd.

Table 2. Dimensions of the planar detector fitted in previous work[1] and those optimized by simulation

parameter	previous	current
h	1 cm	1 cm
r	1.25 cm	1.25 cm
h_1	2.04 μm	3.2 μm
r_1	1.25 cm	1.25 cm
h_2	0.23 cm	0.2 cm
r_2	0.802 cm	0.802 cm
h_3	0.769796 cm	0.79968 cm
r_3	0.928 cm	0.928 cm

The column 'previous' shows results from the simulation published in the reference.[1]
The column 'current' shows the results obtained with the model simulated in this work.

whose intensities were normalized to achieve a total probability equal to 1 for each isotope. The simulated peak intensities found in the tallied pulse height spectra were rescaled after the simulation using the corresponding experimental x-intensity or gamma-intensity to obtain the peak efficiencies. With the results obtained from the six simulations using the dimensions derived from the Seltzer model, the optimized set of dead layer dimensions was derived, and a new set of six simulations was run.

In all simulations, the absorption energies for photons, electrons, and positrons were set in all materials to 1 keV. `WCC` and `WCR` were also set to 1 keV everywhere. The value assigned to the parameters `C1` and `C2` was 0.01, which renders a nearly detailed simulation. For `DSMAX`, the suggestion of the authors of PENELOPE was followed, and the value given to each body was one 10th of its thickness.[9] No variance-reduction technique was used in the simulations other than the restriction of the emitted photons in the forward direction limited by the aforementioned cone.

In every simulation, we tallied the spectrum of the deposited energy in the active germanium volume, which consists of the crystal volume excluding the dead layers. In other words, the energy deposited in the dead layers did not contribute to the tallied quantity. In all simulations, the number of histories was sufficiently high to reduce the standard statistical uncertainty to less than 0.01% in the simulated efficiencies.

The efficiency values deduced from the spectra simulated by PENELOPE must be corrected for the restriction in the semi-aperture of the source solid angle, θ_{sa}. Hence, the efficiency for each energy E_i, $\epsilon_{sim,i}$, is related to the ratio between simulated full-energy events to number of histories of photons of energy E_i, $P_{sim,i}$, by the equation

$$\epsilon_{sim,i} = P_{sim,i}\frac{1-\cos\theta_{sa}}{2}. \quad (1)$$

Results and discussion

The peak efficiencies obtained in the initial set of six simulations were compared with the experimental data. Figure 2 compares the experimental efficiency values with those calculated by simulation and the analytical model, and Table 2 shows the main detector parameters used in the two procedures. It can be seen

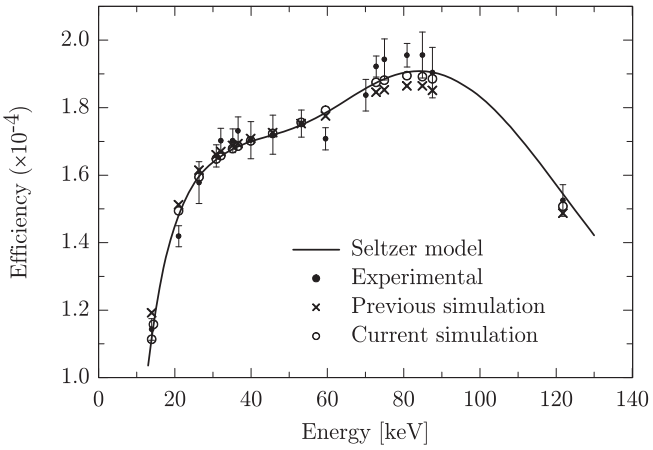

Figure 2. Efficiency of the uncollimated detector as a function of photon energy. The filled circles are experimental values obtained with calibrated radioactive sources: ^{133}Ba, ^{152}Eu, ^{241}Am (Amersham), ^{57}Co and ^{137}Cs from Laboratório de Metrologia Nuclear-Instituto de Pesquisas Energéticas e Nucleares, Comissão Nacional de Energia Nuclear, São Paulo, and their uncertainty bars correspond to one standard deviation. The fitted calibration curve[1] is shown with a line. Simulated efficiencies with the parameters on Table 2 are represented with crosses ('previous') and open circles ('current').

that the efficiencies in the low-energy region are overestimated, whereas in the high-energy region, they are underestimated. Nevertheless, the discrepancies were small, and only two iterations in the process of modifying the dead layer thickness were required to reach a good fit. These iterations consisted of estimating the changes in thicknesses in the thin and thick dead layers that would reproduce the experimental values. A new set of simulations run these modified values. This process was repeated twice until a satisfactory agreement was reached. The simulated values with the current parameters, shown in Table 2, are displayed by open circles in Figure 2.

Note that we had fitted the four parameters of the analytical model to the experimental efficiency values:[1] the central and intermediate radius and the two dead layer thicknesses that correspond to these regions. When simulating the efficiency, just changes in the dead layer thicknesses with respect to the analytical model fitted values were required for a good fit, and we did not verify whether changes in the radius of the two regions would have similar effects on the efficiency curve. Because the simulation and the analytical model eventually yielded almost identical efficiency curves, it was not needed to make a detailed investigation on all parameters.

The restriction to photon source emission in a beam towards the detector, both in the simulation and Seltzer's model, precludes from accounting for photon scattering in the source, which yields a shoulder located at left of the peak, relatively important at these low energies.[13,14] Hence, in our previous analysis,[1] the peak areas were extracted from the experimental spectra as the total number of counts above the continuum part of the spectrum minus the contribution from the components of the response function that extended under the full-energy peak, which represented about 2% of the total peak areas.

The simulation fits the experimental efficiency as well as the analytical model, as expected, although with altered dead layer thicknesses. One of the differences between the methodologies

Copyright © 2015 John Wiley & Sons, Ltd.

is that the analytical model assumed normal photon incidence, while in the simulation, the photons hit the crystal surface with an angle, which is in general not normal to this surface. This explains well the slightly thinner toroidal dead layer (change of 0.03 cm in h_2) required in the simulation, but not the thicker central dead layer. This last difference likely arises from the fact that Seltzer's model deduces the bulk of photon absorption in the detector crystal using attenuation coefficients that do not include coherent scattering. Although it fits better the detector efficiency, it also corresponds to an increased proportion of Compton scattering events that reduces a little bit the efficiency, which may have been compensated by the thinner central dead layer. Therefore, the simulation model, with the dead layers shown in last column of Table 2, can likely be applied to smaller source to detector distances while the analytical model will probably fail.

In the detector model, the inclusion of Ge dead layers, characterized as completely unresponsive regions that attenuate the photon beam, was sufficient to explain the detection efficiency in the energy region of interest (11 keV $< E <$ 150 keV) within the uncertainty of the experimental data. More accurate comparisons between experiments and simulation should consider more complex models that incorporate incomplete charge collection regions. These type of regions have been already mapped in Si detectors[15] and suggested in large volume HPGe detectors.[16,17] In the detector described in the present work, we observed an efficiency loss near the edge of the detector. This phenomenon could be due to a transition layer similar to that proposed by the Majorana collaboration.[18] However, the observed loss of efficiency[1] was small when compared with the experimental uncertainties.

Conclusion

The analytical model proposed by Seltzer can be used to determine the structure and dimensions of the dead layers present in a HPGe planar detector. The results obtained from the analytical model can be used as an initial ansatz for a Monte Carlo simulation of radiation transport in the detector. Following this approach, the dimensions of the dead layers can be adjusted in the simulation, and a very good fit between the simulated and experimental detector efficiency data could be obtained.

A large source-to-detector distance seems to be an important requisite for the validity of the analytical model. With the large source-to-detector geometry used in the calibration showed here, the assumption of normal incidence of the Seltzer's model was acceptable.

Acknowledgements

The authors are thankful to the financial support from the Deutsche Forschungsgemeinschaft (project BR 4043-1/1) and FAPESP (Fundação de Amparo à Pesquisa do Estado de São Paulo, Brazil) contract number 2010/52616-7. L. B. acknowledges support from the Spanish Ministerio de Economía y Competitividad (project FIS2012-38480). N. L. M and V. R. V are grateful also to Brazilian funding agencies CNPq (Conselho Nacional de Desenvolvimento Científico e Tecnológico) and CAPES (Coordenação de Aperfeiçoamento de Pessoal de Nível Superior).

References

[1] N. L. Maidana, V. R. Vanin, V. Jahnke, J. M. Fernández-Varea, M. N. Martins, L. Brualla, *Nucl. Instrum. Meth. A* **2013**, *729*, 371–380.
[2] S. M. Seltzer, *Nucl. Instrum. Methods* **1981**, *188*, 133–151.
[3] A. Elanique, O. Marzocchi, D. Leone, L. Hegenbart, B. Breustedt, L. Oufni, *Appl. Radiat. Isotopes* **2012**, *70*, 538–542.
[4] R. Luís, J. Bento, G. Carvalhal, P. Nogueira, L. Silva, P. Teles, P. Vaz, *Nucl. Instrum. Meth. A* **2010**, *623*, 1014–1019.
[5] S. Carson, C. Iliadis, J. Cesaratto, A. Champagne, L. Downen, M. Ivanovic, J. Kelley, R. Longland, J. R. Newton, G. Rusev, A. P. Tonchev, *Nucl. Instrum. Meth. A* **2010**, *618*, 190–198.
[6] R. G. Helmer, J. C. Hardy, V. E. Iacob, M. Sanchez-Vega, R. G. Neilson, J. Nelson, *Nucl. Instrum. Meth. A* **2003**, *511*, 360–381.
[7] J. M. Fernández-Varea, V. Jahnke, N. L. Maidana, A. A. Malafronte, V. R. Vanin, *J. Phys. B* **2014**, *47*, 155201.
[8] M. M. Bé, V. Chisté, C. Dulieu, Table of radionuclides (Comments on evaluation), **1999**. http://www.nucleide.org/DDEP_WG/DDEPdata.htm (accessed December 23, 2014).
[9] F. Salvat, J. M. Fernández-Varea, J. Sempau, *Penelope 2011—A Code System for Monte Carlo Simulation of Electron and Photon Transport*, OECD Nuclear Energy Agency, Issy-les-Moulineaux, France, **2011**.
[10] J. Baró, J. Sempau, J. M. Fernández-Varea, F. Salvat, *Nucl. Instrum. Meth. B* **1995**, *100*, 31–46.
[11] J. Sempau, E. Acosta, J. Baró, J. M. Fernández-Varea, F. Salvat, *Nucl. Instrum. Meth. B* **1997**, *132*, 377–390.
[12] J. Sempau, A. Badal, L. Brualla, *Med. Phys.* **2011**, *38*, 5887–5895.
[13] M. Majer, M. Budanec, G. Jerbić-Zorc, S. Pasić, M. Uroić, B. Vuković, K. Ilakovac, *Nucl. Instrum. Meth. A* **2004**, *524*, 227–235.
[14] M. Majer, M. Uroić, T. Bokulić, S. Pasić, B. Vuković, K. Ilakovac, *Nucl. Instrum. Meth. A* **2005**, *555*, 243–250.
[15] F. Scholze, F. Procop, *X-Ray Spectrom.* **2009**, *38*, 312–321.
[16] H. Utsunomiya, H. Akimune, K. Osaka, T. Kaihori, K. Furutaka, H. Harada, *Nucl. Instrum Meth. A* **2005**, *548*, 455–463.
[17] N. L. Maidana, L. Brualla, V. R. Vanin, J. R. B. Oliveira, M. A. Rizzutto, E. do Nascimento, J. M. Fernández-Varea, *Nucl. Instrum Meth. A* **2010**, *615*, 285–294.
[18] E. Aguayo, M. Amman, F. T. Avignone, A. S. Barabash, P. J. Barton, J. R. Beene, F. E. Bertrand, M. Boswell, V. Brudanin, M. Busch, Y. D. Chan, C. D. Christofferson, J. I. Collar, D. C. Combs, R. J. Cooper, J. A. Detwiler, P. J. Doe, Y. Efremenko, V. Egorov, H. Ejiri, S. R. Elliott, J. Esterline, J. E. Fast, N. Fields, P. Finnerty, F. M. Fraenkle, A. Galindo-Uribarri, V. M. Gehman, G. K. Giovanetti, M. P. Green, V. E. Guiseppe, K. Gusey, A. L. Hallin, R. Hazama, R. Henning, E. W. Hoppe, M. Horton, S. Howard, M. A. Howe, R. A. Johnson, K. J. Keeter, M. F. Kidd, A. Knecht, O. Kochetov, S. I. Konovalov, R. T. Kouzes, B. D. LaFerriere, J. Leon, L. E. Leviner, J. C. Loach, Q. Looker, P. N. Luke, S. MacMullin, M. G. Marino, R. D. Martin, J. H. Merriman, M. L. Miller, L. Mizouni, M. Nomachi, J. L. Orrell, N. R. Overman, G. Perumpilly, D. G. Phillips, A. W. P. Poon, D. C. Radford, K. Rielage, R. G. H. Robertson, M. C. Ronquest, A. G. Schubert, T. Shima, M. Shirchenko, K. J. Snavely, D. Steele, J. Strain, V. Timkin, W. Tornow, R. L. Varner, K. Vetter, K. Vorren, J. F. Wilkerson, E. Yakushev, H. Yaver, A. R. Young, C. H. Yu, V. Yumatov, *Nucl. Instrum Meth. A* **2013**, *701*, 176–185.

Copyright © 2015 John Wiley & Sons, Ltd.